Acta Oncologica Vol. 35, No. 7, pp. 857–862, 1996

MODELLING OF INITIAL EVENTS AND CHEMICAL BEHAVIOUR OF SPECIES INDUCED IN DNA UNITS BY AUGER ELECTRONS FROM ^{125}I, ^{123}I AND CARBON

EKKEHARD POMPLUN, MICHEL TERRISSOL and MATHILDE DEMONCHY

Auger electron spectra for ^{123}I and ^{125}I generated by Monte Carlo calculation and Auger electrons emitted from carbon after photoelectric effect on its K-shell as well as two DNA models (linear plasmid and nucleosome model) based on x-ray diffraction experiments have been used to simulate the behaviour of all species and radicals created during the physical and the chemical phase of the Auger's transport. By introducing appropriate assumptions for the induction of strand breaks the number of these breaks can also be determined and correlated to experimentally found numbers of lethal events. Efficiency differences between the iodine nuclides themselves and in comparison with the rather monoenergetic Auger electrons from carbon are shown with regard to the direct and indirect effects on the two DNA models. The characteristic products in the physical, chemical and biochemical phase are compared with corresponding results from the literature for low-LET radiation.

Low energy Auger electrons released from DNA-bound ^{125}I have been of increasing interest in radiobiological research since their large biological effect (1, 2) and their potential application to tumour therapy (3) had been demonstrated in the 1970s. In the following years several attempts were made to explain the high radiotoxicity of the Auger emitters. By Monte Carlo simulation (4, 5) the electron spectra of ^{125}I and ^{123}I were generated revealing a shower of very low energy electrons, depositing their energy in the nearest vicinity of the decay site. The utilization of track structure codes and the development of DNA target structures were started by Charlton (6) determining the range of the induced high-LET effect. The combination of electron spectra, track structures and target models allowed to trace the fate of single electrons in spatial relation to critical biological structures. Strand break induction had been simulated (7) and by introducing a target model with atomic resolution (8) the distinction between direct and indirect effects in the simulation became possible.

The track structure code used in this work (9) has been continuously improved, e.g., by introducing active DNA sites and, furthermore, the linear DNA plasmid target structure (8) has been developed to a nucleosome model to be closer to cellular DNA conditions. All calculated numbers of single strand breaks (ssb) and double strand breaks (dsb) as well as the spatial distribution of ssb in linear DNA show reasonable values when compared with experimental data (10). Meanwhile, a complex model consisting of different computer codes is now available being a powerful tool for the elucidation of the radiation action mechanisms in general (11) since low energy electrons play a major role—as primary or higher order particles—in nearly all kinds of radiation. To have a source of those electrons inside the critical biological target facilitates the simulation and statistical counting procedures.

The environment of DNA in the cell consists of water species (close sheaths and bulk water), various proteins

Received 11 September 1995.
Accepted 15 May 1996.
From the Abteilung Sicherheit und Strahlenschutz, Forschungszentrum Jülich GmbH, Jülich, Germany (E. Pomplun) and CPAT, Université Paul Sabatier, Toulouse Cedex, France (M. Terrissol, M. Demonchy).
Correspondence to: Ekkehard Pomplun, Abteilung Sicherheit und Strahlenschutz, Forschungszentrum Jülich GmbH, D-52425 Jülich, Germany.
Paper presented at the Third International Symposium on Biophysical Aspects of Auger Processes, August 24–25, 1995, Lund, Sweden.

 ISSN 0284-186X

and ions. Under irradiation, a variety of species is created and chemical reactions and exchanges become complex. To distinguish the damage induced by direct effects from the one produced via radicals and chemical exchange processes, experimentators and modellers use a simple procedure: by addition of scavengers radicals become neutralized so that—according to the scavenger's concentration—the indirect effect will be more or less suppressed. In this case the resulted damage can be associated with the direct effects.

In simulation studies (8), direct and indirect effects can been distinguished with respect to the geometrical point of the primary ionization. If that point lies inside the DNA target volume a direct effect is assumed, otherwise an indirect one. It is the main focus of this work to simulate the influence of radical scavengers on the radiation effect. Furthermore, the results are used for a comparison of some characteristic products' yields during the different phases of the radiation action followed after application of low-LET radiation and after decay of Auger emitters. As electron sources, besides ^{125}I, also ^{123}I and a single 274 eV electron typically released after K-shell ionization of C-atoms have been taken.

Material and Methods

The simulation model is schematically presented in Fig. 1. Inside a liquid water environment a virtual sphere (working sphere, WS) surrounds the nucleosome. The size of the working sphere (r = 12 nm) has been chosen empirically to fulfil the conditions of, on the one hand, being large enough to include all possible reactions between radicals and DNA and, on the other, to be small enough to still get manageable CPU times for running the model on the computer. The nucleosome is built (11) as a double helix of DNA with 146 bp and 9 056 atoms, surrounding the histones which are considered as energy absorbing but chemically inactive. The electron emission positions are assumed on the thymidine methyl groups replaced by the iodine isotopes. All the nucleosome atoms are known by their co-ordinates and their van der Waals radii.

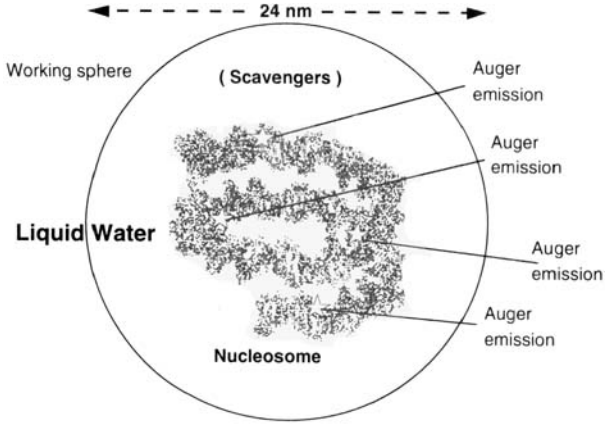

Fig. 1. Schematic presentation of the simulation model.

Details of calculations have been given previously (10–13). Briefly, Monte Carlo simulated ^{125}I and ^{123}I cascades are used as input to a 4-dimensional (x, y, z, t) electron transport in liquid water. At places of double helix atoms, liquid water with density 1.3 is assumed. Complete transport of Auger electrons is then simulated decay by decay in the nucleosome and in the working sphere filled with liquid water of normal density (see Fig. 1).

During the physical step (up to 10^{-15} s) an ionization located inside the van der Waals radius of a phosphate- or sugar-group atom is stored (time, co-ordinates and energy deposited on this atom) as a direct ssb, and this event is removed from the initial track. Then, molecules of scavengers (DMSO here) are added randomly (according to the desired concentration) inside the WS. For a concentration of e.g. 1 M, about 1 290 molecules of scavengers are considered. An average of 180 species is present per ^{125}I decay inside the working sphere at 10^{-12} s (excluding the histone's volume).

The fate of the track is further traced from 10^{-12} s to seconds. All species (e^-_{aq}, $OH^\bullet$, $H^\bullet$, $H3O^+$, H_2O_2, OH^-, H_2, HO_2) and scavengers diffuse according to the Smoluchowski law; about 40 reactions are considered: well-known reactions of water species among themselves as well as reactions with scavengers and sub-units. The reaction of a deoxyribose-monophosphate during this chemical phase leads to its transformation to a subproduct (in this case an indirect ssb is scored with time, co-ordinates and total energy deposited in the working sphere by the Auger electrons belonging to one decay). Dsb is defined per iodine decay or per electron as two ssb on opposite strands within a distance of up to 10 basepairs.

Results and Discussion

The Auger electrons initiate a chain of complex processes in the DNA and its immediate environment starting with ionizations and excitations, production of radicals and induced DNA damages. This development involves a time scale covering many orders of magnitude (from less than a femtosecond to weeks).

Energy deposition and ionizations

For the three different sources of radiation simulated here the energy deposited per decay in spherical shells of 0.1 nm thickness is given for about the whole range (Fig. 2). The curves for the iodine nuclides reflect the different parts of the electron emission spectra (4, 5). The nearly parallel progress of both curves results from the same Auger transitions inside the tellurium. The region up to about 10 nm radius that covers approximately the whole nucleosome receives a nearly constant amount of energy

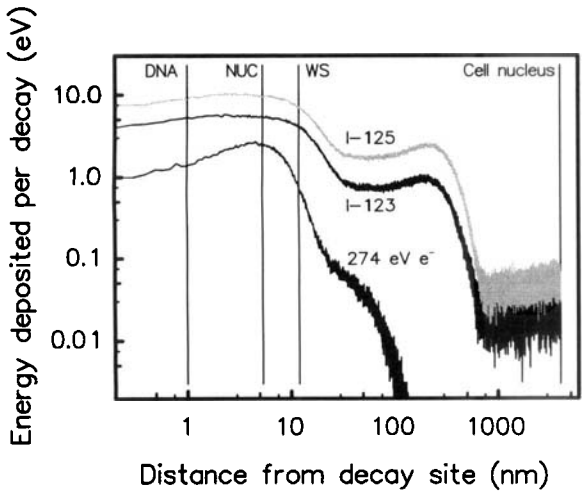

Fig. 2. Energy deposited by ^{125}I, ^{123}I, and the 274 eV electron in spherical shells (logarithmic scale presentation up to geometrical dimensions corresponding to cell nucleus).

deposited by the many Auger electrons below 500 eV. The broad scattering beyond 0.8 μm is caused by the conversion electrons to L- and higher shells as well as by the Auger electrons from transitions to K-shell and the thereof resulting energy and range straggling. The curve for the 274 eV electron shows that the maximum deposition is in dimensions of nucleosome and nearly all is deposited in the working sphere, and so the efficiency for DNA damage will be maximal relatively to energy released. The vertical bars indicate the approximate geometrical size of the biological structures of interest and of the working sphere.

Relating the effectiveness to the total kinetic energy released per decay, differences between the radiation sources become evident. Although the total energy released by the iodine isotopes is approximately the same (Table 1), the energy deposited by ^{125}I in the cell- and DNA-structures is about two times larger than that of ^{123}I. The 274 eV carbon Auger electron—having only 1.5% of the total ^{125}I kinetic energy—causes ionizations in the working sphere and in the nucleosome corresponding to about 20 and 23% of those induced by ^{125}I respectively. It could be stated that the 274 eV electron—representing also the low-energy tail of the iodine Auger spectra—is by far the most effective radiation. This agrees with former investigations about the effectiveness of the Auger electrons with energies below 500 eV (8). Due to the comparable small range of the 274 eV electron, this efficiency increases with decreasing size of the volume considered since the high energy electrons from the Auger spectra may escape from the smaller volumes.

Radical production as a function of scavenger concentration

A specific aspect of the used track structure code lies in its ability to simulate the processes of radical production caused by the initiated ionizations and excitations and, furthermore, to trace the fate of these radicals. Since indirect effects play a major role in radiation-induced damage, the knowledge and understanding of the radiolytic component in the overall effect are of great importance. To validate this part of the simulation code, the number of primary radicals has been calculated as a function of different concentrations of DMSO. About 10^{-9} s after radiation emission, 1M DMSO cleans up all OH so that these radicals will no longer damage the DNA helix. This explains why experimentalists choose DMSO concentrations between 1 and 2 M to hide late indirect effect.

Strand breaks

The numbers of directly induced ssb found here are 1.4, 0.8, and 0.3 for ^{125}I, ^{123}I, and the 274 eV electron respec-

Table 1

Energy released per decay and number of ionizations produced by the three radiation modalities (absolute and relative to ^{125}I decay) in different cellular volumes

	^{125}I Decay	^{123}I Decay	274 eV e^-
Average energy released (keV)	18.01	21.04	0.274
Energy per decay relative to ^{125}I (%)	100	117	1.5
Number of Ionizations			
Cell nucleus (r = 4 μm)			
absolute	454	189	11
relative to ^{125}I (%)	100	42	2.4
Working sphere (r = 12 nm)			
absolute	51	29	10
relative to ^{125}I (%)	100	57	20
Nucleosome (r = 5.5 nm)			
absolute	6.0	3.3	1.4
relative to ^{125}I (%)	100	55	23

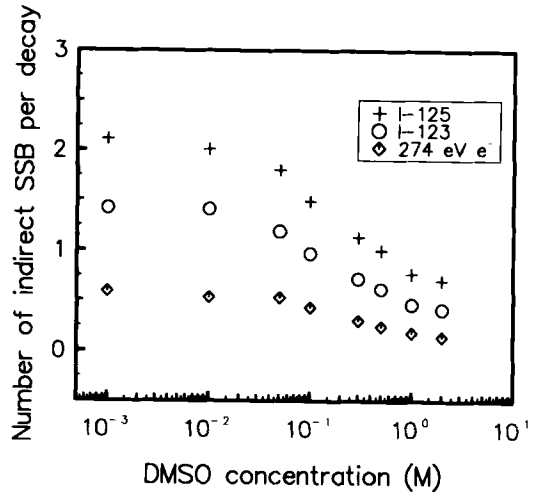

Fig. 3. Number of indirectly induced ssb as a function of DMSO concentration.

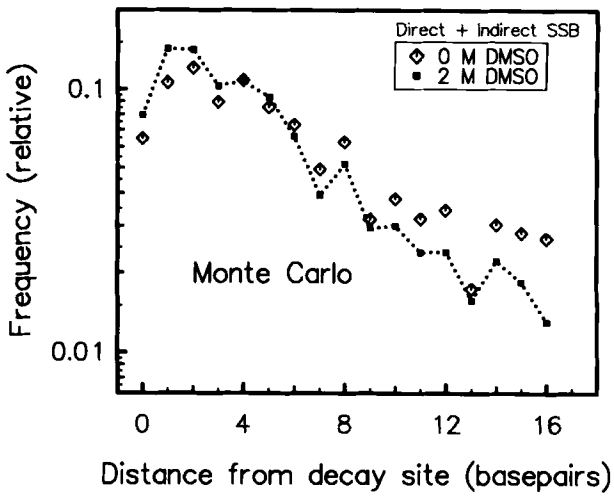

Fig. 4. Spatial distribution of ssb after ^{125}I decay in linear DNA plasmid with 0 and 2 M DMSO concentration (Monte Carlo simulation).

tively. Fig. 3 shows the results for indirectly induced ssb as a function of DMSO concentration. For the no-scavenger situation we found 2.1 indirect ssb per ^{125}I decay which adds up with the 1.4 directly induced ones to a total number of 3.5 ssb per decay of this nuclide. This is less than 4.2 ssb found in a previous study (11), the difference being due to the fact that the influence of the histons has been taken into account absorbing all radicals entering the histons' volume. Nevertheless, the value of 3.5 ssb per ^{125}I decay is still inside the range of experimental data between 3 and 6 ssb per decay (14–16). However, the number of dsb simulated here as 0.65 per decay seems to be low compared with experimental values of 1.0 (17) and 0.9 (18).

Of particular interest is the number of ssb obtained with 0.5 M DMSO for which also an experimental value is reported by Feinendegen et al. (14) who found 6.0 ssb per ^{125}I decay for no-scavenger and 4.0 ssb for 4% DMSO (about 0.5 M). This DMSO concentration means a reduction of ssb to 0.66 of the no-scavenger value. The same ratio (0.68) has been found in this work (2.4 ssb at 0.5 M DMSO against 3.5 ssb at 0.0 M DMSO), so that there is a strong indication that the simulation of the scavenger behaviour is reasonable (see Table 2).

Table 2

Number of single strand breaks per decay of ^{125}I for no-scavenger and for 0.5 M DMSO

DMSO concentration (M)	Experiment (Feinendegen et al., 1977)	MC simulation (this work)
0.0	6.0	3.5
0.5	4.0	2.4
Reduction rate (%)	33	31

The spatial distribution of strand breaks after ^{125}I decay in linear plasmid DNA has been investigated experimentally (19) and theoretically (7, 12, 10). (For details of the experimental set-up and of the simulation technique see the referenced papers). From the results given in Fig. 4, it can be seen that at larger distances from the decay site the indirect effect is responsible for the strand breakage. The curve for the 2 M DMSO simulation reflects a situation approximately free of radicals and representative for the ssb induction by direct effects. This is confirmed by Fig. 5, showing no difference between the results for directly induced ssb and the total number of ssb; i.e., 2 M DMSO suppresses ssb production via radicals.

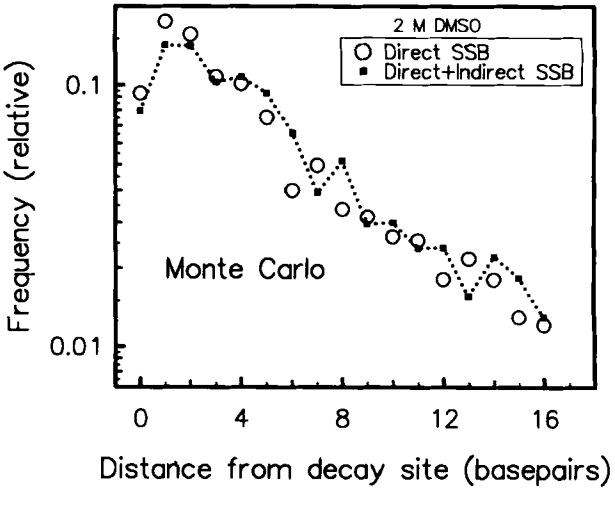

Fig. 5. Spatial distribution of ssb (total number versus number of directly induced ssb) after ^{125}I decay in linear DNA plasmid for 2 M DMSO concentration (Monte Carlo simulation).

Table 3

Products in a mammalian cell nucleus after application of 1 Gy low-LET radiation (see (20)) and after ^{125}I radiation yielding about comparable cellular effects

Products	1 Gy low-LET-radiation	50 decays of ^{125}I inside DNA[d]
Initial events (physical phase)		
Ionizations in the cell nucleus	~100 000[a]	~23 000
Excitations in the cell nucleus		~12 000
Ionizations in the DNA	~2 000[a]	~300
Excitations in the DNA	~2 000[a]	~130
Radicals in the cell nucleus (after 10^{-12} s)		
$OH^{\bullet}$	~85 000[c,d]	~32 000
e^-_{aq}	~80 000[c,d]	~25 000
$H^{\bullet}$	~27 000[c,d]	~14 000
DNA damages		
Single strand breaks	1 000[b]	~200
Double strand breaks	40[b]	~40–50
Cellular effects		
Lethal events	~0.2–0.8[a]	~1[e]

[a] (20)
[b] (21)
[c] estimated by G-values taken from (22)
[d] this work
[e] (23)

Auger electrons and low-LET radiation

To give an overall characterization of the Auger electron irradiation of cell nuclei in terms of consequences for the different phases of the radiation action the product's yields have been compiled together with comparable values for low-LET irradiation (Table 3). The ^{125}I data are scaled in such a way that the probability of cell death equals unity. This allows an approximate comparison between both irradiation modalities. The assumption of 50 ^{125}I decays inside the DNA necessary to induce cell death is based on different experimentally found D_0-values ranging from 28 for human lymphoblast cells (24), 46 for mouse leukaemic cells (23) to 91 decays for human T cells (3). The yield of ionizations by the iodine Auger electrons in the cell nucleus is only about one-fifth of the low-LET value, the ionizations in the DNA being reduced even by a factor of about seven. Assuming a dsb as being created by two neighbouring ssb, the ^{125}I ssb are five times more efficient in the dsb production (0.2 dsb/ssb) than the low-LET radiation (0.04 dsb/ssb). An obvious explanation for this difference would be the fact that the range of energy deposition and in consequence of ionizations and of ssb are much closer in the Auger emitter case.

To conclude, this work deals mainly with the simulation of the influence by DMSO on the indirect radiation effect induced by DNA-incorporated Auger electron emitters. Concentrations of more than 1 M DMSO scavenge nearly all OH radicals, leading to a significant decrease in ssb production. The reduction rate is in good agreement with experimental values. A comparison between a no-scavenger situation and a 2 M DMSO application shows that ssb induction relatively far away from the electron source is mainly mediated via radicals. To study more efficiently low and very low scavenger concentrations it would be preferable to simulate external irradiation (e.g. from ^{137}Cs) able to produce more homogeneous inchoative OH distributions than with Auger electron emitters. The presented data are based on a model still in progress. It is intended to extend the nucleosome model to the chromatine fiber and to simulate radiation transport in the complex environment of the cell nucleus.

REFERENCES

1. Feinendegen LE, Ertl HH, Bond VP. Biological toxicity associated with the Auger effect. In: Ebert H, ed. Proceedings of the Symposium on Biophysical Aspects of Radiation Quality. Vienna: IAEA, 1971: 419–30.
2. Hofer KG, Hughes WL. Radiotoxicity of intranuclear tritium, iodine-125 and iodine-131. Radiat Res 1971; 47: 94–109.
3. Feinendegen LE. Biological damage from the Auger effect, possible benefits. Radiat Environ Biophys 1975; 12: 85–99.
4. Pomplun E, Booz J, Charlton DE. A Monte Carlo simulation of Auger cascades. Radiat Res 1987; 111: 533–52.
5. Pomplun E. ^{123}I: Calculation of the Auger electron spectrum and assessment of the strand breakage efficiency. In: Howell RW, Narra VR, Sastry KSR, Rao DV, eds. Biophysical aspects of Auger processes, Woodbury, NY: American Institute of Physics, 1992: 121–36.
6. Charlton DE. The range of high LET effects from ^{125}I decays. Radiat Res 1986; 107: 163–71.
7. Charlton DE, Humm JL. A method of calculating initial DNA strand breakage following the decay of incorporated ^{125}I. Int J Radiat Biol 1988; 53: 353–65.

8. Pomplun E. A new DNA target model for track structure calculations and its first application to I-125 Auger electrons. Int J Radiat Biol 1991; 59: 625–42.
9. Terrissol M, Beaudré A. Simulation of space and time evolution of radiolytic species induced by electrons in water. Radiat Prot Dosim 1990; 31: 175–7.
10. Terrissol M, Pomplun E. Computer simulation of DNA-incorporated ^{125}I Auger cascades and of the associated radiation chemistry in aqueous solution. Radiat Prot Dosim 1994; 52: 177–81.
11. Pomplun E, Terrissol M. Low-energy electrons inside active DNA models: a tool to elucidate the radiation action mechanisms. Radiat Environ Biophys 1994; 33: 279–92.
12. Pomplun E, Roch M, Terrissol M. Simulation of strand break induction by DNA-incorporated ^{125}I. In: Howell RW, Narra VR, Sastry KSR, Rao DV, eds. Biophysical aspects of Auger processes. Woodbury, NY: American Institute of Physics, 1992: 137–52.
13. Terrissol M. Modelling of radiation damage by ^{125}I on a nucleosome. Int J Radiat Biol 1994; 66: 447–51.
14. Feinendegen LE, Henneberg P, Tisljar-Lentulis G. DNA strand breakage and repair in human kidney cells after exposure to incorporated iodine-125 and cobalt-60 γ-rays. Current Topics in Radiation Research Quarterly 1977; 12: 436–52.
15. Sundell-Bergman S, Johanson KJ. Repairable and unrepairable DNA strand breaks induced by decay of ^{3}H and ^{125}I incorporated into DNA of mammalian cells. Radiat Environ Biophys 1980; 18: 239–48.
16. Painter RB, Young BR, Burki HJ. Non-repairable strand breaks induced by ^{125}I incorporated into mammalian DNA. Proc Natl Acad Sci USA 1974; 71: 4836–8.
17. Krisch RE, Krasin F, Sauri CJ. DNA breakage, repair, and lethality accompanying ^{125}I decay in microorganisms, Current Topics in Radiation Research Quarterly 1977; 12: 355–68.
18. LeMotte PK, Little JB. DNA damage induced in human diploid cells by decay of incorporated radionuclides. Cancer Res 1984; 44: 1337–42.
19. Martin RF, Haseltine WA. Range of radiochemical damage to DNA with decay of iodine-125. Science 1981; 213: 896–8.
20. Goodhead DT. Initial events in the cellular effects of ionizing radiations: clustered damage in DNA. Int J Radiat Biol 1994; 65: 7–17.
21. Ward JF. DNA damage produced by ionizing radiation in mammalian cells: identities, mechanisms of formation and reparability. Prog Nucleic Acid Res Mol Biol 1988; 35: 95–125.
22. Beaudré A. Simulation spatio-temporelle sur ordinateur des processus radiolytiques induits dans l'eau par des électrons. (Dissertation) l'Université Paul Sabatier, Toulouse, No. 371, 1988 (in French).
23. Burki HJ, Roots R, Feinendegen LE, Bond VP. Inactivation of mammalian cells after disintegrations of ^{3}H or ^{125}I in cell DNA at -196°C. Int J Radiat Biol 1973; 24: 363–75.
24. Liber HL, LeMotte PK, Little JB. Toxicity and mutagenecity of x-rays and [I-125] dUrd or [H-3]TdR incorporated in the DNA of human lymphoblast cells. Mutat Res 1983; 111: 387–404.